JMEPEG (2011) 20:1401–1413
DOI: 10.1007/s11665-010-9786-y

1059-9495/$19.00

Filament-Level Modeling of Aramid-Based High-Performance Structural Materials

M. Grujicic, W.C. Bell, P.S. Glomski, B. Pandurangan, C.-F. Yen, and B.A. Cheeseman

(Submitted October 2, 2010)

Molecular statics and molecular dynamics are employed to study the effects of various microstructural and topological defects (e.g., chain ends, axial chain misalignment, inorganic solvent impurities, and sheet stacking faults) on the strength, ductility, and stiffness of *p*-phenylene terephthalamide (PPTA) fibers/filaments. These fibers can be considered as prototypes for advanced high strength/high-stiffness fibers like Kevlar®, Twaron®, New Star®, etc. While modeling these fibers, it was taken into account that they are essentially crystalline materials consisting of stacks of sheets, with each sheet containing an array of nearly parallel hydrogen-bonded molecules/chains. The inter-sheet bonding, on the other hand, was considered as mainly being of van der Waals or p-electron character. The effects of various deviations of the PPTA fiber structure from that of the perfectly crystalline structure (i.e., microstructural/topological defects) on the material's mechanical properties are then considered. The results obtained show that while the presence of these defects decreases all the mechanical properties of PPTA fibers, specific properties display an increased level of sensitivity to the presence of certain defects. For example, longitudinal tensile properties are found to be most sensitive to the presence of chain ends, in-sheet transverse properties to the presence of chain misalignments, while cross-sheet transverse properties are found to be most affected by the presence of sheet stacking faults.

Keywords filament-level modeling, Kevlar, microstructural defects, topological defects

1. Introduction

High specific-strength (i.e., strength normalized by density) and high specific-stiffness (i.e., stiffness normalized by density) polymer-based fiber/filament materials (e.g., Kevlar®, Twaron®, New Star®, etc.) are commonly used in various protective systems whose main requirement is a high level of penetration resistance against high kinetic energy projectiles (e.g., bullets, mine, (Improvised Explosive Device) IED or turbine fragments, etc.). The fibers/filaments are normally used as either thread constituents in two-or three-dimensional woven fabric structures or as reinforcements in high-performance (typically) polymer-matrix composites. The high mass-efficiency (i.e., mass-normalized performance) makes these materials and structures particularly suitable for use in applications such as protective garments for personnel extremity protection, interior spall liners in infantry vehicles, and a lining/shroud for turbine-fragment containment.

Traditionally, the development of the protection systems described above is carried out almost entirely using legacy knowledge and extensive fabrication/testing *trial-and-error* approaches. This approach is not only economically unattractive but is often associated with significantly longer lead times. Consequently, this purely empirical approach has gradually become complemented by the appropriate cost- and time-efficient computer-aided engineering analyses. This trend has been accelerated by the recent developments in the numerical modeling of transient non-linear dynamics phenomena such as those accompanying blast and ballistic loading conditions. In particular, recent advances have enabled the coupling between Eulerian solvers (used to model gaseous detonation products and air) and Lagrangian solvers (used to represent solid components of the protection systems as well as projectiles). It is well recognized that the lack of maturity of the computer-aided engineering analyses in the context of composite material-based protection systems is predominantly due to the inability of currently available material models to realistically represent the response of these materials under high-deformation rate, large-strain, high-pressure loading conditions, the conditions typically encountered during projectile impact events. In this study, an attempt is made to provide a tangible contribution to remedying some of the short-comings of this composite-material models.

Modeling of either the fabric-based structures/materials or of the composite materials reinforced with such structures is very challenging due to (a) the associated multi-length scale hierarchical nature of these materials/structures; (b) the complex nature of the nonlinear, time-dependent mechanical response of the attendant materials; and (c) the multiplicity and complexity of the accompanying phenomena/processes (e.g., filament twisting, interfilament friction, sliding, etc.). To help clarify the nature of the multi-length-scale hierarchy of the fabric structures or fiber-reinforced composite materials, a set of simple schematics and explanations is provided in Fig. 1. The first column in this figure shows a set of simple schematics of the material microstructure/architecture at a given length-scale along with the labels used to denote the main microstructural

M. Grujicic, W.C. Bell, P.S. Glomski, and **B. Pandurangan**, Department of Mechanical Engineering, Clemson University, Clemson, SC 29634; and **C.-F. Yen** and **B.A. Cheeseman**, Army Research Laboratory – Weapons & Materials Research Directorate Aberdeen, Proving Ground, MD 21005-5069. Contact e-mail: gmica@clemson.edu.

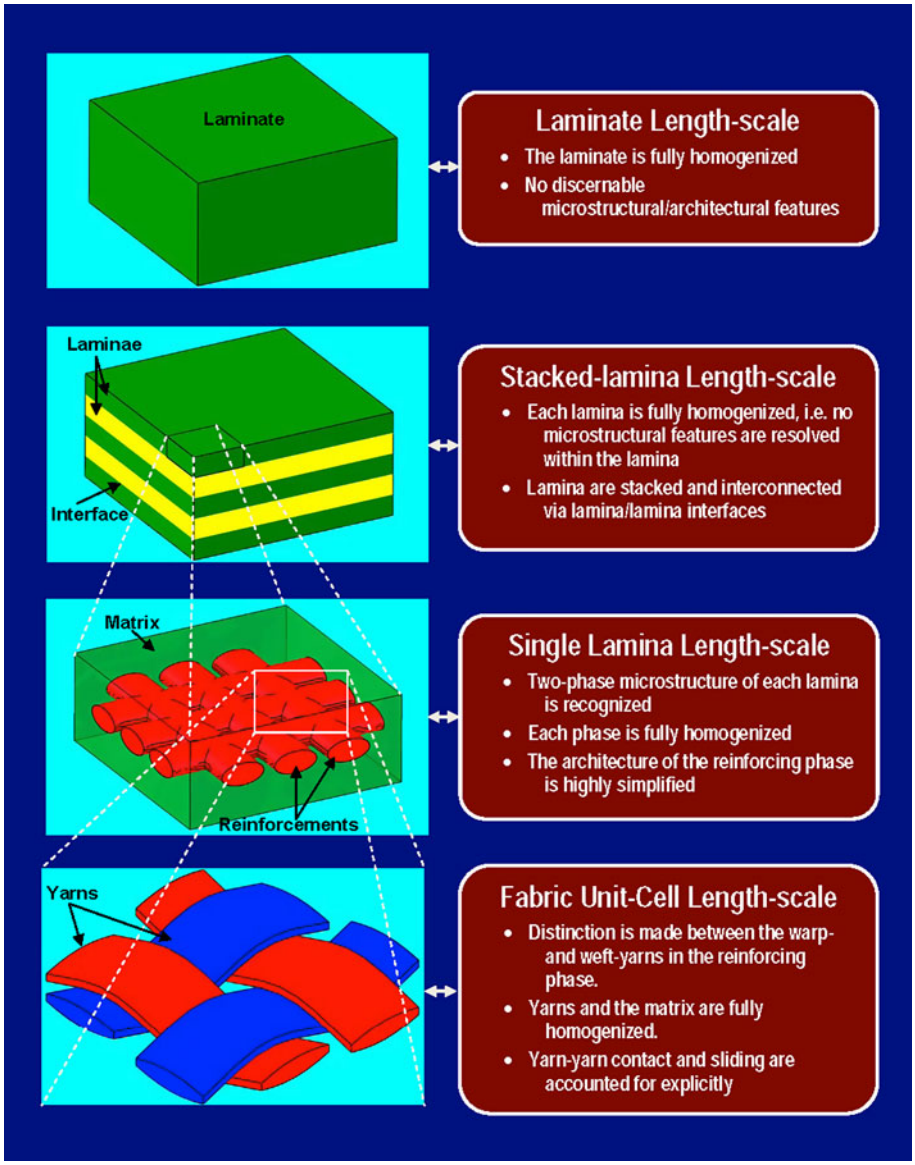

Fig. 1 Various length-scales and the associated material model assumptions/simplifications used in the study of polymer-matrix composite materials with high-performance fiber-based structures

constituents. In the second column, a brief description is provided of the material models used to capture the material behavior at the length-scale in question. A brief description of the material microstructure/architecture and the corresponding material models at each of the length-scales listed in Fig. 1 is provided below:

Laminate length-scale: At this length-scale, the material is completely homogenized, i.e., there are no discernable microstructural features in the material. An example of the laminate-length scale composite material model can be found in Ref 1.

Stacked-lamina length-scale: At this length-scale, the material is modeled as a stack of fully homogenized laminae, adjoined along (also fully homogenized) lamina/lamina interfaces. An example of the composite material model at this length-scale can be found in Ref 2.

Single-lamina length-scale: In this case, the microstructure/architecture of the reinforcement and matrix phases are explicitly taken into account and separate material models are used for the two lamina constituents within a micromechanics computational approach. The resulting "*two-phase*" composite-lamina model for each lamina is then combined with a fully homogenized lamina/lamina interface model to form a stacked-lamina composite laminate structure. An example of this type of material model can be found in Ref 3.

Fabric unit-cell length-scale: At this length-scale, a closer look is given to the architecture of the woven fabric. Specifically, details of yarn weaving and crimping, yarn cross-sectional change, and yarn sliding at the warp-yarn/weft-yarn cross-over points are taken into account. Each yarn is fully homogenized in this case as are the matrix and the lamina/lamina interfaces. An example of the model of this type can be found in Ref 4-6.

Yarn length-scale: In this case, the internal structure/architecture of each yarn is accounted for explicitly. Specifically, yarns are considered as assemblies of nearly parallel

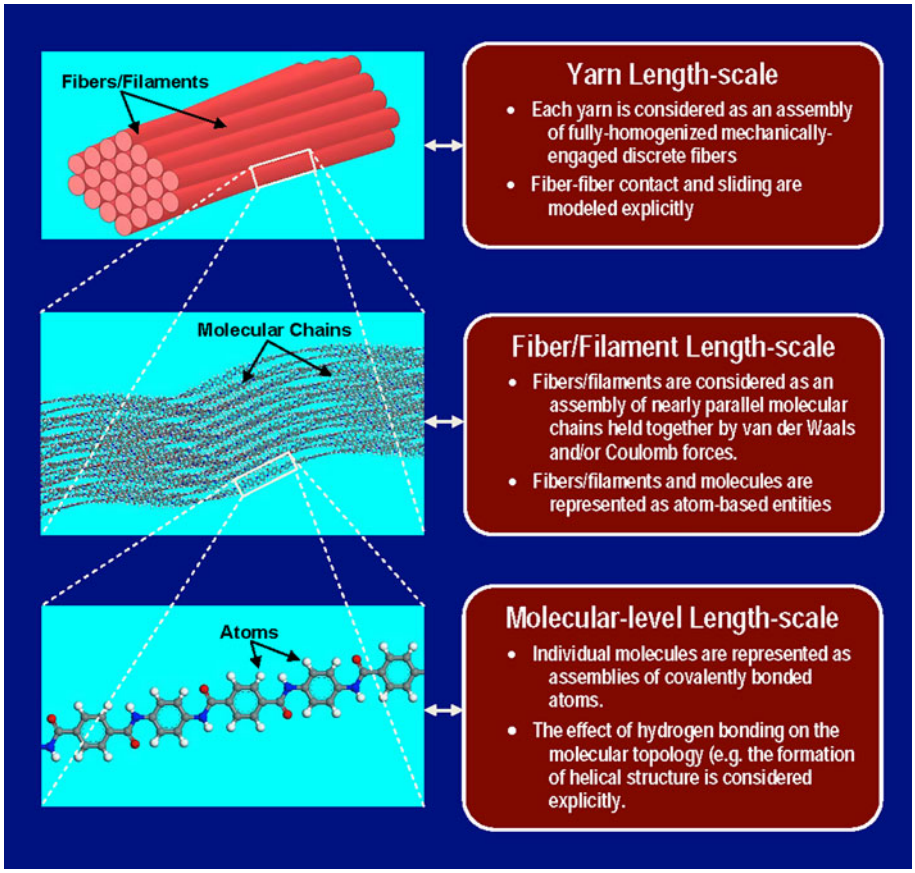

Fig. 1 Continued

fibers/filaments which are mechanically engaged by either the application of a light twist to the yarn or by wrapping a fiber around the fiber/filament assembly. Typically, the detailed microstructure of the yarns is not incorporated into material models used in large-scale simulations of projectile/protection-system impact interactions (due to the unmanageably large computer resources needed). Instead, computational results of the mechanical response of the individual yarns, when subjected to a variety of loading conditions, are used to enrich the yarn material model formulation which is, in turn, used at the fabric unit-cell length scale. An example of this approach can be found in Ref 7.

Filament/fiber length-scale: At this length-scale, fibers are considered as assemblies of aligned long-chain molecules which are held together by non-bond (van der Waals or Coulomb) forces. It is this length-scale that is the subject of this investigation. At this length-scale, molecules are treated as collections of covalently bonded atoms. In other words, the filaments are modeled using an atomistic/molecular approach within which the constituent particles (atoms or ions) interact via valence-bond and non-bond forces. As in the previous case, the knowledge gained at this length-scale is used to enrich the material description at the next layer length-scale (the filament length-scale, in this case) and is not directly used in the large-scale modeling of projectile/particle structure interactions.

Molecular-level length-scale: At this length-scale, chemical structure and conformation of the individual molecules constituting the chain are analyzed using the aforementioned atomic/molecular modeling tools/procedures. The main goal of the analysis at this length-scale is to identify the most-likely molecular conformations present in the filaments. This greatly reduces the computational cost expended at the fiber length-scale. This is the reason that this length-scale is also the subject of this study.

The main objective of this study is to establish the effect of various microstructural and topological molecular/fiber-level defects on the mechanical properties of *p*-phenylene terephthalamide (PPTA) filaments. These types of filaments can be considered as a generic form of the commercial aromatic polyamide/aramid fibers such as Kevlar®, Twaron®, New Star®, etc. Owing to the fine length-scale of the problem at hand, this analysis will employ molecular-level simulation methods and tools (i.e., molecular statics and molecular dynamics). However, the results obtained can be used to augment material models describing the material behavior at coarser (e.g., yarn, fabric, etc.) length-scales. Unfortunately, coarser length-scale material model augmentation is beyond the scope of this study. The main reasons for this are as follows: the extent to which this augmentation should be carried out is dependent on the likelihood of presence of different defects. Such likelihood is expected to be greatly affected by the specificities related to the polymer chemistry, polymer synthesis and fiber/yarn/fabric fabrication processes. Such details are not available in this study.

The organization of the paper is as follows: a brief overview of the PPTA (i.e., generic Kevlar®) fiber/filament chemistry,

single-chain conformations and multi-chain assemblies into sheets and three-dimensional crystals is presented in section 2. Molecular-level computational procedure including the computational cell construction, force-field identification, computational method(s) selection, microstructural/topological defects generation and the problem definition are respectively presented in section 3.1-3.5. The key results obtained in this study are presented and discussed in section 4. A summary of the study carried out and the key results/conclusions are given in section 5.

2. Fundamentals of Kevlar Fibers

Kevlar® (*p*-phenylene terephthalamide, PPTA) belongs to the family of polymeric materials known as polyamides. Polyamides are typically classified as aromatic polyamides or aramids (e.g., Kevlar®, Twaron®, New Star®, etc.) and non-aromatic polyamides (e.g., Nylon 6,6). A sketch of the Kevlar® single repeat unit is displayed in Fig. 2(a). It consists of two amide linkages

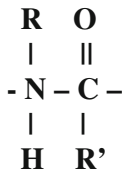

connecting two (R=R′=C_6H_4) phenylene rings/moieties. For clarity, the atomic species are labeled in Fig. 2(a). While, in principle, Kevlar® can appear both in the *trans*- (Fig. 2a) and *cis*- (Fig. 2b) stereo-isomeric conformations, the *trans* conformation is almost exclusively found. In Latin, *trans*- and *cis*-denote "*opposite*" and "*on the same side*", respectively. It should be noted that due to the fact that the "*all-trans*" molecular configuration results in the formation of extended/stretched-out molecules (which, in turn, enable the fibers consisting of large numbers of nearly parallel molecules to take full advantage of the back-bone covalent bonds and to crystallize), this configuration is preferred. The aforementioned finding of the *all-trans* molecular conformation can be readily understood by analyzing Fig. 2(b), which shows clear evidence of *steric hindrance*/spatial interference between the hydrogens attached to the two phenylene moieties (Ref 8-11).

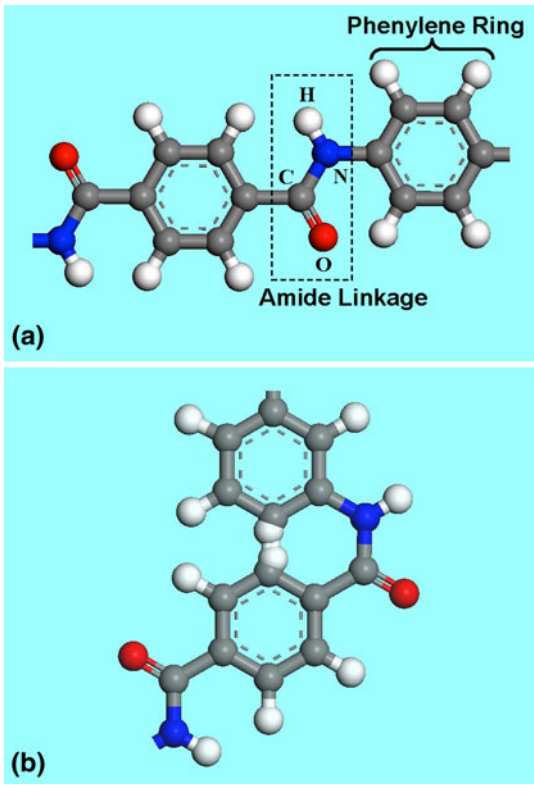

Fig. 2 (a) *trans*- and (b) *cis*-molecular conformations in typical aramid-based polymeric-material chains/molecules

Owing to a large difference in electronegativity between oxygen and hydrogen, amide linkages act as strong electrically charged dipoles. The resulting strong hydrogen bonding causes: (a) the formation of a helical structure of the Kevlar® chains; and (b) lateral bonding between the parallel Kevlar® chains which results in the formation of "*sheet-like*" structures. While PPTA fibers are commonly found to have a crystalline structure consisting of stacked sheets, hydrogen bonding does not make a significant contribution to the inter-sheet bonding. It should be noted that the sheets are not entirely planar but contain pleats (known to be on a length scale of hundreds of nanometers). Thus, pleats are beyond the length scale of features that are accounted for explicitly in this molecular-level investigation; they will become apparent at the next higher length scale.

During the spinning process, the crystalline structure orients itself in such a way that the chain's axis is aligned with the spun fiber axis. The presence of a large fraction of the crystalline phase and the molecular alignment along the filament axis are responsible for the desirable combination of properties of Kevlar® fibers which can be summarized as follows: (a) high absolute and normalized stiffness and tenacity/strength (e.g., Kevlar is five times stronger than steel and while its density is approximately one half that of fiberglass); (b) superior abrasion resistance; (c) high creep resistance; (d) low thermal and mechanical conductivity; (e) good high-temperature stability. The maximum service temperature is ca. 150-170 °C; (f) high melting point. In fact, degradation of the molecular structure that initiates at temperatures around 500 °C typically precedes melting; (g) low flammability; and (h) high resistance to organic solvents. In addition, the presence of hydrogen bonding and a crystalline phase is responsible for some of the observed deficiencies in this class of materials such as: (a) relatively low elongation at break (~3.5%); (b) pronounced sensitivity to acids and salts; (c) enhanced sensitivity to ultraviolet radiation; and (d) high tendency for static-charge build-up.

Kevlar® is available in a number of fiber grades such as: (a) Kevlar® 29; (b) Kevlar® 49; (c) Kevlar® 100; (d) Kevlar® 119; (e) Kevlar® 129; (f) Kevlar® AP; and (g) Kevlar® XP™. Different grades of Kevlar® are tailored toward specific applications. For example, Kevlar® 119 possesses a relatively high flexibility, enhanced total elongation and high fatigue resistance and is, hence, used in automotive tires, serpentine-belts and high-pressure hoses. On the other hand, Kevlar® 129 and Kevlar® XP™ are optimized for high tenacity and are, hence mainly used in personnel ballistic vests and helmets, vehicle flexible-armor structures, etc. While all these Kevlar® grades differ in the details of their chemical composition, molecular structure and conformation, and synthesis/processing conditions, they are essentially aromatic polyamides. Consequently, the generic aromatic polyamide (PPTA) single-chain molecular-level structure depicted in Fig. 2(a) (as well as the

associated multi-chain structures obtained by agglomeration of nearly parallel chains) will be used as a prototype for all the aforementioned Kevlar® grades.

PPTA chains are inherently stiff and hence the chains do not readily form kinks and jogs. Consequently, in contrast to the flexible polymeric molecules which can undergo extensive folding and form the common (crystalline + amorphous) two phase structure, the PPTA fibers tend to typically form either a *para*-crystalline or a fully crystalline structure. Tendency for the formation of *para*-crystalline or crystalline structures is promoted by the presence of the planar phenylene and amide groups and by the ability of the adjacent chains to form hydrogen bonds. In the case of the *para*-crystalline structure, PPTA molecules are all aligned in the same direction but no order exists in a plane orthogonal to this direction. In sharp contrast, in the case of the fully crystalline PPTA fibers, molecules are aligned in all three mutually orthogonal directions.

As will be discussed in greater detail in the next section, the PPTA crystal structure is layered and consists of parallel (ABABAB…) stacked sheets. As stated earlier, the sheets are formed due to hydrogen bonding between the adjacent parallel PPTA molecules. The inter-sheet bonding on the other hand is mainly of the van der Waals and p-electron type. Owing to the relatively low strength of the van der Waals and the p-electron type inter-sheet bonding, PPTA fibers are prone to the formation of stacking faults and kink bands, and typically possess an inferior compressive strength and buckling resistance.

As discussed above, PPTA fibers are generally considered as crystalline materials. However, this picture is highly idealized and the real PPTA fibers contain a variety of crystallographic and microstructural imperfections or defects. In accordance with standard practice, these defects are classified as: (a) point defects (e.g., chain ends, inorganic-solvent impurities, etc.); (b) line defects (e.g., misaligned molecules); and (c) planar defects (e.g., sheet stacking faults). It is well established that the presence of such defects can greatly (and generally adversely) affect the mechanical properties of the PPTA fibers. In this study, an attempt is made to assess the extent of sensitivity of material strength, ductility and stiffness to the presence of these defects. This was accomplished by carrying out a series of molecular-level calculations using "*perfectly-crystalline*" and "*defective*" PPTA-based structures.

PPTA fibers/filaments are fabricated using the so-called "*dry jet wet spinning*" process. Within this process, PPTA is first converted into a low-viscosity liquid crystalline solution (commonly referred to as "*dope*") containing only 5-20 wt.% of polymer. The solution is next extruded/spun into filaments and stretched prior to entering a warm-water coagulation bath. Because of the liquid crystalline nature of the dope, polymer molecules are forced into alignment as they flow through spinneret orifice with further alignment occurring during stretching. The coagulated fibers are washed, dried, and heat treated under tension to reduce the concentration of microstructural and topological defects and to further improve the molecular alignment. Clearly, the quality (as measured by the chemical purity and extent of crystalline perfection) of the processed PPTA fibers is affected by the dry jet-wet spinning process parameters as well as by the quality of the precursor materials and the polymer synthesis process. For example, due to the non-uniform nature of coagulation, it is likely that dry jet-wet spun fibers (in particular the core section of the fibers) may contain void-like imperfections which are highly detrimental to the fiber strength, ductility and stiffness.

3. Molecular-Level Computational Procedure

As mentioned earlier, molecular-level computational methods have been employed in this study in order to investigate the effect of various imperfections/defects on the mechanical properties of aromatic polyamides. Within these methods, all atoms and bonds are explicitly accounted for and molecular mechanics, dynamics, or Monte Carlo algorithms are used to quantify the behavior of the material under investigation.

While ab initio quantum mechanics methods have the advantage over the molecular-level methods since they do not require parameterization, they have a serious short-coming. Namely, due to prohibitively high computational cost, they can be currently employed only for systems containing no more than a few hundred atoms/particles. As will be shown below, while ab initio quantum mechanics calculations are not directly used in this study, some of the computational ab initio quantum mechanics results are used in the parameterization of the material model at the molecular length/time scale. Utility of the molecular-level computational results is greatly dependent on accuracy and fidelity of the employed force-field (the mathematical expression which describe various bonding and non-bonding interaction forces between the constituents of the molecular-scale model). In this study, the so-called "*COMPASS*" (Condensed-phase Optimized Molecular Potentials for Atomistic Simulation Studies) force-field is used (Ref 12, 13). This highly accurate force-field is of an ab initio type since most of its parameters were determined by matching the predictions made by the ab initio quantum mechanics calculations to the condensed-matter experimental data. Hence, it should be recognized that the COMPASS force-field is a prime example of how the highly accurate results obtained on one length/time scale (quantum mechanical/electronic, in this case) and the experimental data can be combined to parameterize material models used at coarser length/time scale (the molecular length/time scale, in this case).

Formulation of a molecular-level simulation problem requires, at a minimum, specification of the following three aspects: (a) a molecular-level computational model consisting of atoms, ions, functional groups and/or molecules; (b) a set of force-field functions; and (c) a computational method(s) to be used in the simulation. More details of these three aspects of the molecular-level modeling and simulations of aromatic polyamides are provided below.

3.1 Computational Model

The first step in the molecular-level computational analysis was the construction of a single PPTA repeat unit. This unit is analogous to the molecular structure displayed in Fig. 2(a), except that the two end bonds are capped with hydrogen. One of the capping hydrogen atoms is denoted as the tail of the repeat unit while the other was designated as the head. This was carried out using the Visualizer (Ref 14) program from Accelrys.

In order to model the behavior of long PPTA chains at the molecular length-scale, the following procedure was employed:

(a) The repeat unit constructed above is first grown by a copy-and-attach process in which the tail of a repeat unit is connected to the head of the adjacent unit and vice versa;

(b) The multiple repeat-unit PPTA chain constructed in (a) is next subjected to a series of back-bone torsions in order to obtain the commonly observed helical topology of the PPTA chains. The values for the specific torsional angles were obtained from Ref 8 and are summarized in Table 1. The values of the back-bone bond angles obtained from Ref 8 are also listed in Table 1. To help with the understanding of the torsional operation employed and with the definition of the back-bone bond angles, a schematic of the PPTA repeat unit is provided in Fig. 3 along with the labels for the torsional and bond angles in question. It should be noted that the multi-repeat-unit PPTA chains are used to construct infinitely long chains through the application of the periodic boundary conditions in the chain-axis direction. To ensure that the chain topology is correctly transferred across the boundary of the adjacent unit cells, the total rotation angle associated with a finite-length multi-repeat-unit chains (equal to a product of the number of the repeat units within a chain and the total rotational angle per repeat unit) had to be set to 360°;

(c) As explained above, to obtain an infinitely long PPTA chain, the periodic boundary conditions are applied to the finite-length multi repeat-unit single (helical) chain along the chain axis. The resulting molecular configuration is optimized by minimizing its potential energy with respect to the positions of the constituent atoms. An example of the molecular-level topology of a single infinitely long chain is depicted in Fig. 4(a);

Table 1 Bond angles and torsion angles used to arrive at the helical PPTA structure

Bond angles	Value, °	Torsion angles	Value, °
C_{ar}-C_{am}(b)-N	118.7 ± 0.3	N-C_{am}-C_{am}-N	−2.7 ± 3.0
C_{ar}(a)-C_{am}=O	120.4 ± 0.4	C_{am}-C_{am}-N-N	4.7 ± 3.1
C_{am}-N-H	117.0 ± 0.8	C_{am}-N-N-C_{am}	−1.8 ± 1.6
C_{am}-N-C_{ar}	126.0 ± 3.3	N-N-C_{am}-C_{am}	−4.5 ± 2.7
C_{ar}-N-H	117.3 ± 1.6	Phenylene (diamine)	15-43(c)
C_{ar}-N-C_{am}	126.0 ± 3.0	Phenylene (di-acid)	16-43(c)
N-C_{am}=O	120.5 ± 0.6		
N-C_{am}-C_{ar}	120.0 ± 1.0		

(a) Part of a phenylene ring. (b) Attached to amide linkage. (c) Rotation out-of-plane of preceding phenylene group

(d) When analyzing the molecular structure/conformation of the PPTA filaments/fibers, one must recognize that each fiber consists of a very large number of, nearly parallel, closely packed molecules. These molecules tend to align in such a way that the resulting structure is crystalline. The structure can be described as consisting of the so-called "*pleated*" and "*parallel-stacked*" sheets. A schematic of the crystalline structure within PPTA fibers is provided in Fig. 5. It should be recognized that a vast majority of the molecules inside a PPTA fiber are fully surrounded by other chains, i.e., most of the molecules experience a bulk-like environment. To account for this fact, the periodic boundary conditions are applied not only in the fiber axial direction but also in the two other transverse directions (one residing within the PPTA sheets while the other being normal to these sheets). In other words, the PPTA is assigned a crystalline structure by defining a unit cell and by applying the periodic boundary conditions across the faces of the cell. The unit cell is assigned a high aspect-ratio prismatic shape and a ca. 30° rhombic base while the long axis of the prism is aligned with the axis of the helical molecules. Typically, two fibers are placed into a single unit cell and the unit cell lateral dimensions adjusted to obtain a target density of 1.5 g/cm^3. Also, typically, the computational cell used in this study contains 896 atoms of carbon, 640 atoms of hydrogen, 128 atoms of nitrogen and 128 atoms of oxygen. The resulting molecular configuration is optimized by minimizing its potential energy with respect to the positions of the constituent atoms. An example of the molecular-level topology of the bulk-like crystalline structure within the infinitely long PPTA fibers is depicted in Fig. 4(b). It should be noted that, for improved clarity, the configuration displayed in Fig. 4(b) contains only two repeat units along the chain directions.

3.2 Force-Fields

As stated above, the behavior of a material system at the molecular-level is governed by the appropriate force-fields which describe, in an approximate manner, the potential energy hyper-surface on which the atomic nuclei move. In other words, the knowledge of force-fields enables determination of the potential energy of a system in a given configuration. In general, the potential energy of a system of interacting particles

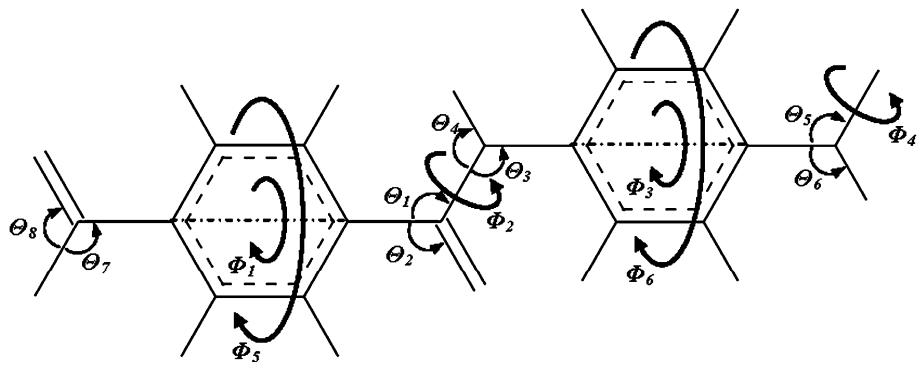

Fig. 3 Definition of eight bond angles, θ_1-θ_8, and six torsion angles, ϕ_1-ϕ_6 used to define the conformation of a single PPTA repeat unit

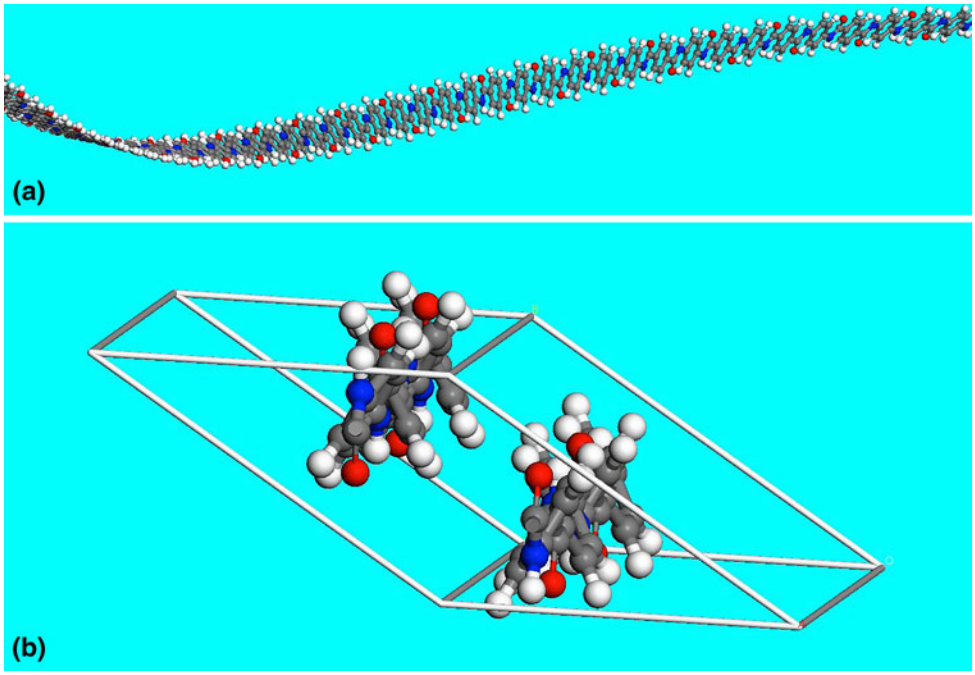

Fig. 4 Typical molecular-level configurations used in this analysis for (a) a single infinitely long PPTA molecule, and (b) for a perfect three-dimensional PPTA crystal

can be expressed as a sum of the valence (or bond), E_{valence}, cross-term, $E_{\text{cross-term}}$, and non-bond, $E_{\text{non-bond}}$, interaction energies as

$$E_{\text{total}} = E_{\text{valence}} + E_{\text{cross-term}} + E_{\text{non-bond}} \quad \text{(Eq 1)}$$

The valence energy generally includes a bond stretching term, E_{bond}, a two-bond angle term, E_{angle}, a dihedral bond-torsion term, E_{torsion}, an inversion (or an out-of-plane interaction) term, E_{oop}, and a Urey-Bradlay term (involves interactions between two atoms bonded to a common atom), E_{UB}, as

$$E_{\text{valence}} = E_{\text{bond}} + E_{\text{angle}} + E_{\text{torsion}} + E_{\text{oop}} + E_{\text{UB}} \quad \text{(Eq 2)}$$

The cross-term interacting energy, $E_{\text{cross-term}}$, accounts for the effects such as bond length and angle changes caused by the surrounding atoms and generally includes: stretch-stretch interactions between two adjacent bonds, $E_{\text{bond-bond}}$, stretch-bend interactions between a two-bond angle and one of its bonds, $E_{\text{bond-angle}}$, bend-bend interactions between two valence angles associated with a common vertex atom, $E_{\text{angle-angle}}$, stretch-torsion interactions between a dihedral angle and one of its end bonds, $E_{\text{end\_bond-torsion}}$, stretch-torsion interactions between a dihedral angle and its middle bond, $E_{\text{middle\_bond-torsion}}$, bend-torsion interactions between a dihedral angle and one of its valence angles, $E_{\text{angle-torsion}}$, and bend-bend-torsion interactions between a dihedral angle and its two valence angles, $E_{\text{angle-angle-torsion}}$, terms as:

$$\begin{aligned} E_{\text{cross-term}} = & E_{\text{bond-bond}} + E_{\text{angle-angle}} + E_{\text{bond-angle}} \\ & + E_{\text{end\_bond-torsion}} + E_{\text{middle\_bond-torsion}} \\ & + E_{\text{angle-torsion}} + E_{\text{angle-angle-torsion}} \end{aligned} \quad \text{(Eq 3)}$$

The non-bond interaction term, $E_{\text{non-bond}}$, accounts for the interactions between non-bonded atoms and includes the van der Waals energy, E_{vdW}, and the Coulomb electrostatic energy, E_{Coulomb}, as

$$E_{\text{non-bond}} = E_{\text{vdW}} + E_{\text{Coulomb}} \quad \text{(Eq 4)}$$

As mentioned earlier, this molecular-level analysis of aromatic polyamide employs the COMPASS (Ref 12, 13) force-field for various bond and non-bond interaction energies appearing in Eq 1-4. A summary of the COMPASS force-field functions can be found in our previous study (Ref 15).

3.3 Computational Method

Both molecular statics and molecular dynamics simulations were employed in this study. Within the molecular statics approach, the unit-cell potential energy (as defined by Eq 1-4) is minimized with respect to the positions of the constituent particles/atoms. The potential energy minimization within Discover (Ref 16) (the atomic simulation program from Accelrys used in this study) is carried out by combining the Steepest Descent, Conjugate Gradient, and Newton's minimization algorithms. These algorithms are automatically deactivated/activated when the atomic configuration approaches its energy minimum (i.e., the Steepest Descent method is activated at the beginning of the energy minimization procedure while Newton's method is utilized in the final stages of this procedure).

Within the molecular dynamics approach, the gradient of the potential energy with respect to the particle positions is first used to generate forces acting on the particles and, then, the associated Newton's equations of motion (for all particles) are integrated numerically in order to track the temporal evolution of the particle positions. Only the equilibrium molecular dynamics method is employed in this study. Within the equilibrium molecular-dynamics method, the system under consideration is coupled to an (external) environment (e.g., constant pressure piston, constant temperature reservoir, etc.) which ensures that the system remains in equilibrium (i.e., the

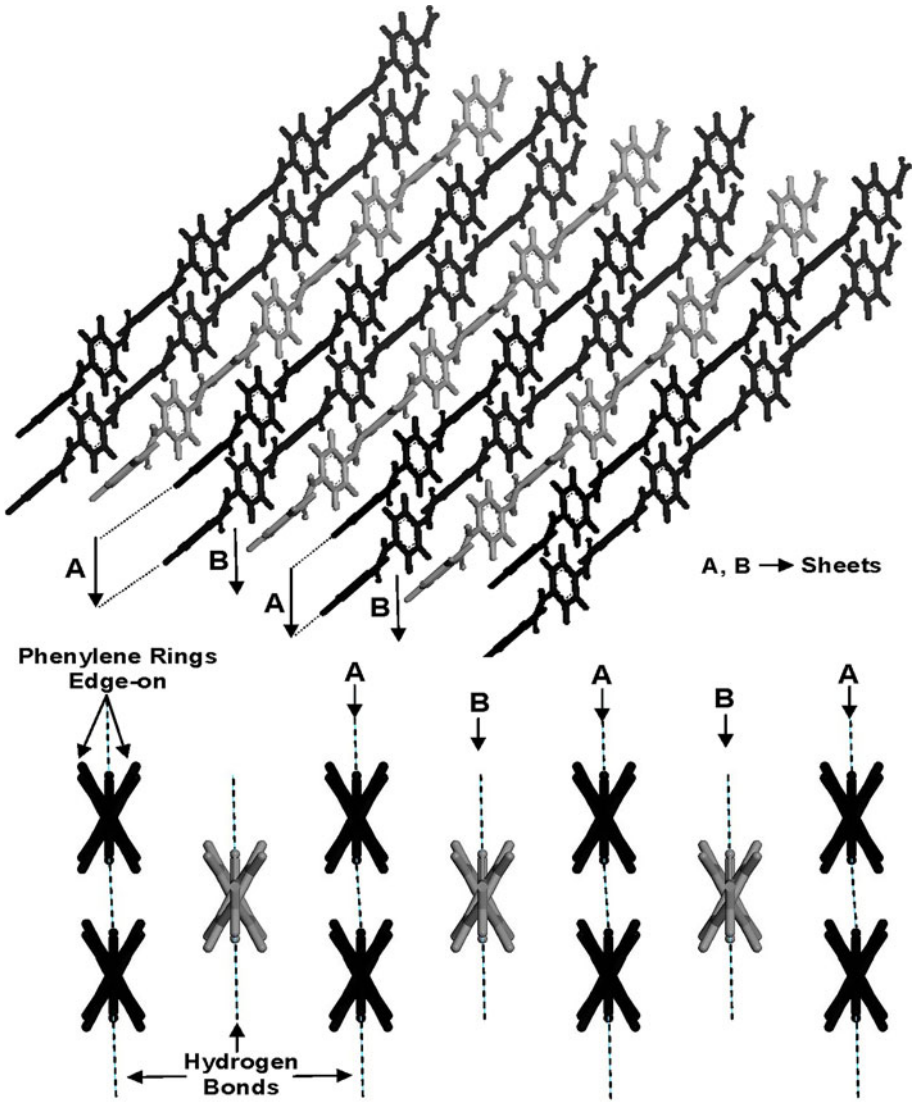

Fig. 5 A schematic of the three-dimensional PPTA crystal structure consisting of parallel hydrogen-bonded PPTA molecules, forming sheets and a perfectly regular ABAB… stacking of these sheets

system is not subjected to any thermodynamic fluxes). In this study, *NVT* and *NσT* equilibrium molecular dynamics simulations are employed (where *N* is the (fixed) number of atoms, *V*, the computational cell volume (also fixed), σ is the (fixed) stress and *T* = (298 K) is the temperature).

3.4 Generation of Defects/Flaws

As discussed earlier, the main objective of this study is to examine, using molecular-level computational methods and tools, the effect of various microstructural and topological defects onto the strength, ductility, and stiffness of PPTA fibers. The defects considered in this study include: (a) point defects (chain ends and inorganic-solvent impurities); (b) line defects (axial chain misalignment); and (c) planar defects (sheet stacking faults). The defects are introduced into the material by either a process involving molecule scission and hydrogen-capping, or by molecule alignment/position modifications. Typical molecular-level microstructures and topologies associated with each of these defects will be presented and discussed in the results section of this article.

3.5 Problem Formulation

The main problem addressed in this study was determination of the strength, ductility and stiffness of the PPTA in either its perfect-crystal configuration or in various defective configurations. The molecular-level procedures used to assess strength, ductility and stiffness of PPTA are described in the remainder of this section.

3.5.1 Strength. Tensile and compressive strengths are determined in three orthogonal (principal) directions by subjecting the unit cell to the appropriate deformation mode and detecting the moment when the rate of stress increase with increase in strain begins to decline appreciably. The mathematical procedure used to compute stress within a molecular length-scale frame is discussed below. The three principal directions are respectively aligned with the overall

direction of the molecules, with an in-sheet direction normal to the first direction and in a direction normal to the sheets.

3.5.2 Ductility. Ductility is quantified as the minimum strain at which complete material separation takes place. Ductility is also analyzed in the three principal directions, but only under tension.

3.5.3 Stiffness. Within the molecular-level computational framework, the components of the fourth-order elastic stiffness tensor are typically determined by employing either a molecular statics approach or a molecular dynamics approach. Within the former approach, the contributions of the finite-temperature thermal expansion and the configurational/vibrational entropic effects to the system free energy are ignored. Consequently, the resulting elastic stiffness tensor defined as a second-order derivative of the system's free energy (i.e., potential energy, in the zero temperature case) with respect to the unit-cell strain components reflects the behavior of the material in question under small deformations at zero absolute temperature. The aforementioned thermal expansion and entropic effects are included within the molecular dynamics based material-stiffness assessment approach. A brief description of the two approaches at hand is provided below.

Molecular Statics Approach. Assessment of the "*static*" elastic stiffness constants of a molecular system in a given configuration is carried out using a total of 13 energy minimization calculations. The first calculation minimizes the energy of the starting molecular configuration. The subsequent 12 calculations are carried out after the unit cell is subjected to either one of the six tensile/compressive uniaxial-strain (small magnitude) deformation modes or to one of the six positive/negative pure shear (small magnitude) deformation modes. For each of the 12 deformation modes, the symmetric second-order stress tensor, σ_{nj}, is obtained from the corresponding optimized configuration by evaluating the (analytical) system virial as:

$$\sigma_{nj} = \frac{1}{V}\left\{\sum_{a>b}\frac{\partial E}{\partial r_{ab}}\frac{(x_{ab})_n(x_{ab})_j}{r_{ab}}\right\} \quad \text{(Eq 5)}$$

where the summation is carried over all *a*-*b* atomic pairs in the unit cell and V is unit cell volume, E is the system potential energy, r_{ab} is the *a*-*b* inter-atomic spacing, and x_a is the position vector of atom a. For each of the 12 deformation modes the associated non-zero components of the elastic stiffness tensor are obtained by dividing each stress component by the respective (non-zero) strain component. Finally, the corresponding elastic stiffness tensor components are averaged for the corresponding tensile/compressive normal and positive/negative simple shear deformation modes.

Molecular Dynamics (Fluctuations) Approach. Within this approach, the elastic stiffness tensor is assessed without subjecting the computational unit cell in question to any of the aforementioned deformation modes. Instead, an extended (equilibrium) molecular dynamics analysis is carried out under preselected constant conditions (e.g., N, number of particles in the unit cell; V, unit cell volume; T, temperature), and the (dynamic-equilibrium fluctuation) results obtained used to assess the time-averaged extent of correlation between the stress and strain components. The stress and strain second-order tensor components are calculated, respectively, as:

$$\varepsilon_{ik} = \frac{1}{2}\left(h_{nl}\langle h\rangle_{lk}^{-1}h_{np}\langle h\rangle_{pi}^{-1} - \delta_{ik}\right) \quad \text{(Eq 6)}$$

$$\sigma_{nj} = \frac{1}{V}\left\{\sum_{a}\frac{(p_a)_n(p_a)_j}{m_a} + \sum_{a>b}\frac{\partial U}{\partial r_{ab}}\frac{(x_{ab})_n(x_{ab})_j}{r_{ab}}\right\} \quad \text{(Eq 7)}$$

where h is a second-order tensor populated by the three vectors making up the unit cell edges, δ is the Kronecker delta, p_a is the momentum of atom a, m is the mass of atom a, and angular brackets are used to denote the time average of a given ensemble quantity.

The components of the elastic stiffness tensor are then calculated using the following equations:

$$C_{iklm} = \frac{k_B T}{\langle V\rangle}\langle\varepsilon_{ik}\varepsilon_{lm}\rangle^{-1} \quad \text{(Eq 8)}$$

$$C_{iklm} = \langle\varepsilon_{ik}\sigma_{nj}\rangle\langle\varepsilon_{nj}\varepsilon_{lm}\rangle^{-1} \quad \text{(Eq 9)}$$

where k_B is the Boltzman's constant, T is the absolute temperature, and $\langle\varepsilon_{ik}\varepsilon_{lm}\rangle$ refers to second moments of the strain fluctuations. Equation 8 and 9 are respectively strictly valid for the constant stress and the constant unit-cell shape (including the volume) ensembles. Using the Voigt notation, the fourth-order stiffness tensor C_{iklm} is converted into a 6×6 elastic stiffness matrix, C. Typically, it was found that the C matrix contains nine independent elements, i.e., that the PPTA crystal structure is orthotropic. Then, using the standard procedure, e.g., Ref 3, the following nine engineering parameters of elastic moduli are determined: the three Young's moduli (E_1, E_2, and E_3), the three shear moduli (G_{12}, G_{13}, and G_{23}), and the three Poisson's ratios (ν_{12}, ν_{13}, and ν_{23}). However, only the effects of the microstructural and topological defects on the Young's Moduli are investigated in this study.

4. Results and Discussion

As discussed earlier, the main objective of this study is to examine the effect of four microstructural/morphological defects on the mechanical properties of PPTA crystalline fibers. The four defects considered in this study include: (a) chain end (a point defect); (b) inorganic-solvent impurity (a point defect); (c) chain misalignment (a line defect); and (d) sheet stacking fault (a planar defect). The mechanical properties of interest include: (a) tensile yield strength; (b) tensile ductility; and (c) stiffness. The effect of each of the defects considered on the mechanical properties is presented in the subsequent four sections. It should be noted that a complete study of the effect of defects on the material properties must include the stochastic nature of the defect population/density. While such a comprehensive study is beyond the scope of this study, it will be addressed in our future communications.

To quantify the effect of these defects, a comparative analysis is carried out involving the corresponding mechanical properties of the defect-free and defective PPTA crystals. The application of the molecular-level computational tools described in the previous section yielded the following rounded mean values of the mechanical properties of the perfect PPTA crystal structure:

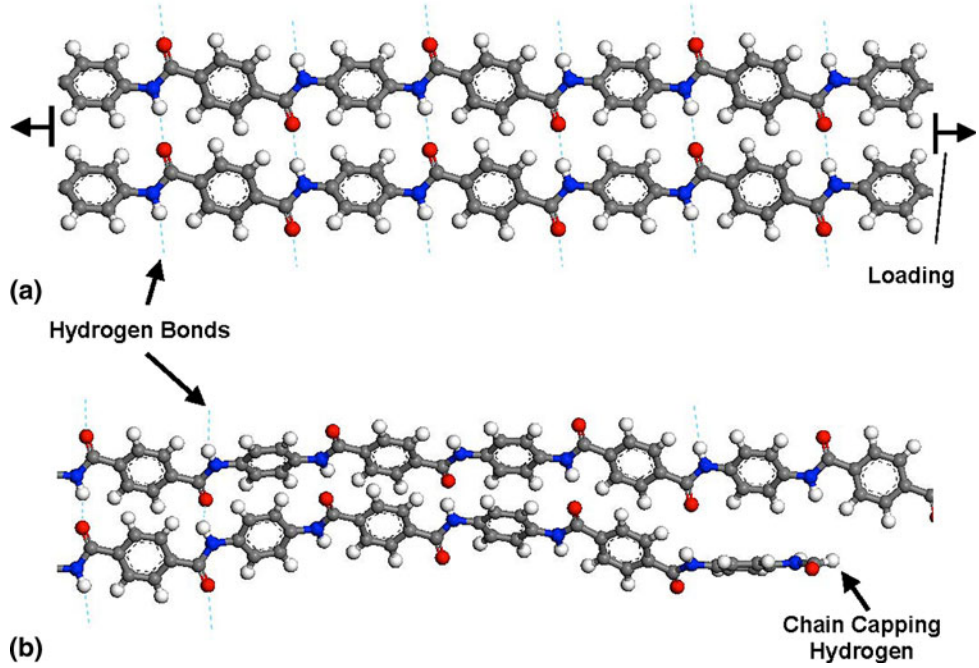

Fig. 6 Prototypical molecular-level computational results of (a) a perfect PPTA crystal, and (b) a PPTA crystal containing a chain end, when subjected to the same tensile longitudinal load

Longitudinal tensile yield strength = 1 GPa;
In-sheet tensile yield strength = 80 MPa;
Cross-sheet tensile yield strength = 45 MPa;
Longitudinal tensile ductility = 4.7%;
In-sheet tensile ductility = 2.5%;
Cross-sheet tensile ductility = 5.0%; and
Three Orthotropic Young's Moduli E_1, E_2, and E_3 in GPa = 190, 15, and 10, respectively.

These values are reasonable when compared to their experimental counterparts observed in commercial fibers like Kevlar® (Ref 17).

Before analyzing the computational data, it was assumed that intra-sheet hydrogen bonding and inter-sheet van der Waals bonding do not make appreciable contributions to the material longitudinal properties. This turned out to be not so, and the longitudinal strength/stiffness values for PPTA crystals were found to be 7-10% higher than their single-chain counterparts. This finding was rationalized as follows: stretching of a single PPTA chain was accompanied by a (laterally) unconstrained rotation of the phenylene rings. Since the same rotation was constrained in the PPTA crystal by the neighboring chains, the resulting material strength/stiffness was increased.

4.1 Chain End

The presence of a chain end within the computational cell is found to predominantly affect the longitudinal (along the chain axis) strength, ductility, and stiffness properties. For the case analyzed here, which involves a relatively high concentration of chain ends (one chain end for every 64 repeat units), the results obtained show that the longitudinal tensile strength is lowered by ca. 6-8% and the longitudinal ductility is lower by ca. 10-12%. On average, the in-sheet and the cross-sheet strength and ductility were affected by less than ca. 5%. The following Young's moduli were obtained in this case: E_1 = 140 GPa, E_2 = 8 GPa, and E_3 = 4 GPa.

An example of the typical molecular-level configuration obtained in this case is displayed in Fig. 6(a) and (b). The results displayed in these figures correspond, respectively, to the case of a perfect PPTA crystal, Fig. 6(a), and a PPTA crystal containing a chain end, Fig. 6(b), both subjected to the same tensile longitudinal strain. Owing to the local disturbance of the perfect crystalline structure and the accompanying loss of the hydrogen bond, the defective crystal is expected to be less strong and stiff. This is indeed the case, as the load supported by the defective crystal in Fig. 6(b) is ca. 25% lower.

4.2 Inorganic-Solvent Impurity

The presence of an inorganic-solvent impurity within the computational cell is found to significantly affect the strength, ductility, and stiffness properties in all the three principal directions. For the case analyzed here which involves a relatively high concentration of inorganic-solvent impurities (five Na_2SO_4 molecules for every 64 repeat units), the results obtained showed that (a) the tensile strengths in the longitudinal, in-sheet, and across sheet principal directions are reduced by ca. 4%, ca. 15%, and ca. 4%, respectively; and (b) tensile ductility properties are reduced by ca. 11%, ca. 3%, and ca. 35%, respectively—while the following Young's moduli were obtained, respectively, in this case: E_1 = 115 GPa, E_2 = 10 GPa, E_3 = 5 GPa.

An example of the typical molecular-level configuration obtained in the above case is displayed in Fig. 7(a) and (b). The results displayed in these figures correspond, respectively, to the statically relaxed molecular configurations of a perfect PPTA crystal, Fig. 7(a), and a PPTA crystal containing five Na_2SO_4 (inorganic-solvent) molecules, Fig. 7(b). An examina-

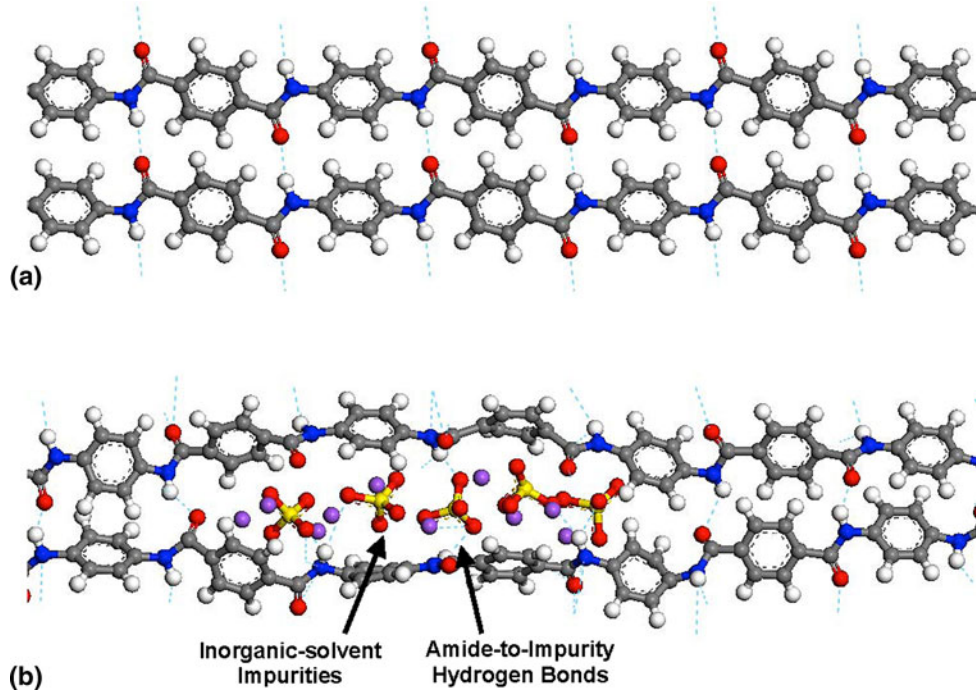

Fig. 7 Prototypical molecular-level computational results of (a) a of a perfect PPTA crystal, and (b) a PPTA crystal containing an inorganic-solvent impurity when subjected to static-relaxation of the molecular configurations

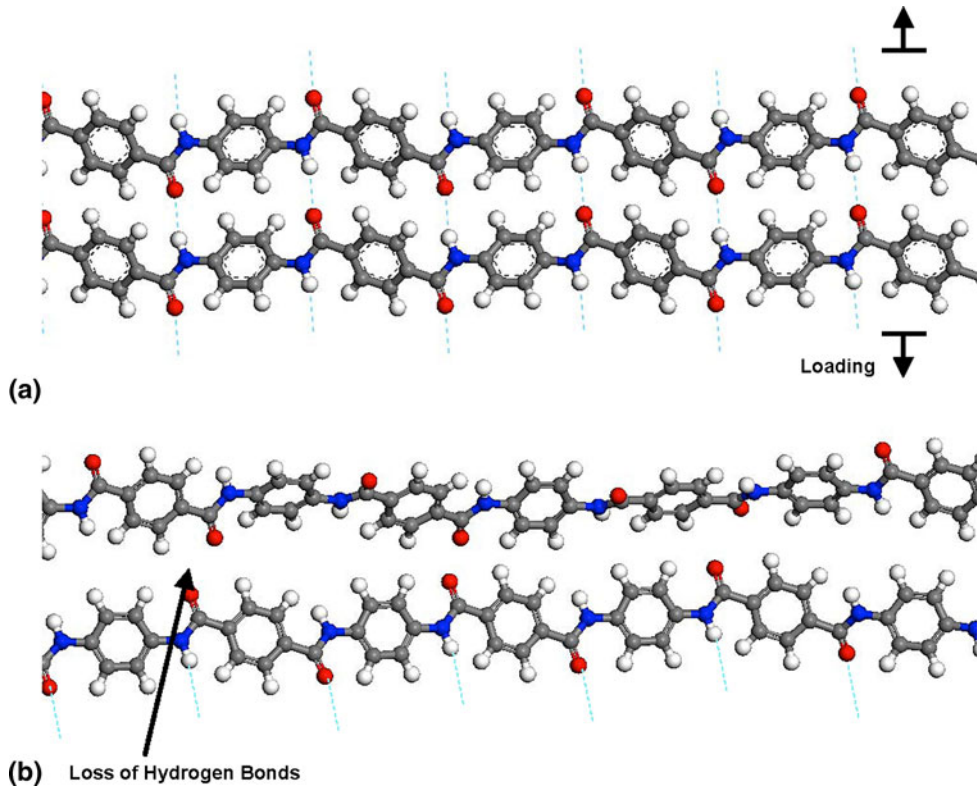

Fig. 8 Prototypical molecular-level computational results of (a) a perfect PPTA crystal, and (b) a PPTA crystal containing a chain misalignment, when subjecting the crystal lattice to tensile in-sheet transverse loads

tion of these figures suggests that due to inter-chain hydrogen bond breaking and disruption of the local crystalline order (chains are displaced radially within the sheet by the solvent molecules, while adjacent sheets are locally distorted around the impurity), the defective crystal has inferior mechanical properties relative to its perfect-crystal counterpart.

4.3 Chain Misalignment

The presence of a chain misalignment within the computational cell is found to mainly affect the in-sheet transverse strength, ductility, and stiffness properties. For the case analyzed here which involves relatively high concentration of chain misalignments (one chain misalignment for every 16 chains), the results obtained show that the in-sheet transverse tensile strength is lowered by ca. 17%, and the in-sheet transverse tensile ductility is lowered by ca. 22%. On average, the longitudinal and the cross-sheet strength and ductility were affected by less than ca. 10%. The following Young's moduli were, respectively, obtained in this case: E_1 = 165 GPa, E_2 = 12 GPa, E_3 = 8 GPa.

An example of the typical molecular-level configuration obtained in this case is displayed in Fig. 8(a) and (b). The results displayed in these figures correspond, respectively, to the case of a perfect PPTA crystal, Fig. 8(a), and a PPTA crystal containing a chain misalignment, Fig. 8(b), both subjected to the same tensile in-sheet transverse load. An examination of these results shows the complete loss of hydrogen bonding in the region of inter-chain misalignment. It is therefore evident that the defective material is less stiff/strong than its perfectly crystalline counterpart in the in-sheet transverse direction.

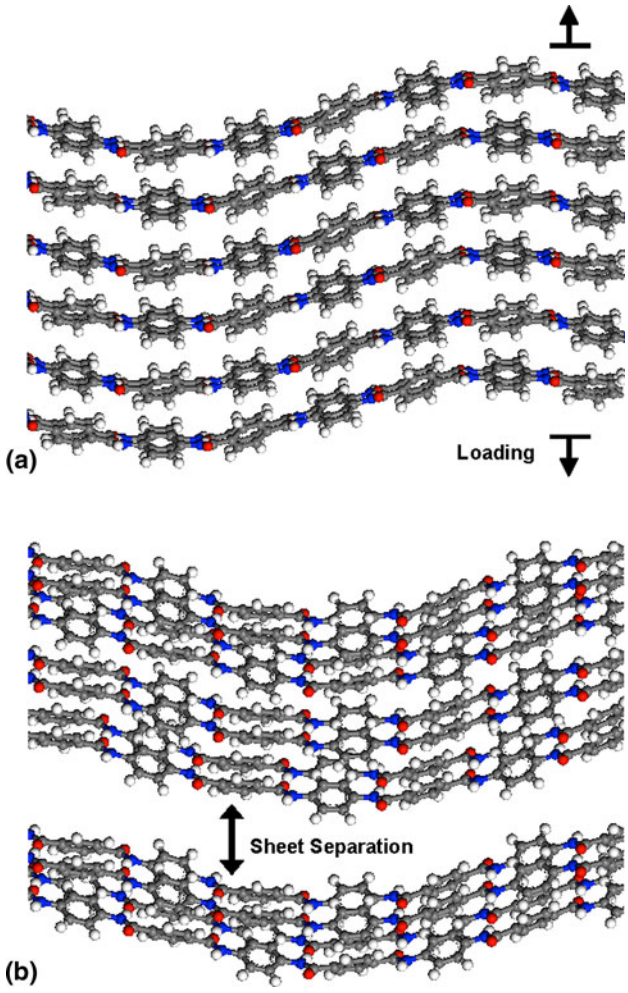

Fig. 9 Prototypical molecular-level computational results of (a) a perfect PPTA crystal, and (b) a PPTA crystal containing a sheet stacking fault, when subjected to cross-sheet transverse tensile load

4.4 Sheet Stacking Fault

The presence of a sheet stacking fault within the computational cell is found to predominantly affect the cross-sheet transverse strength, ductility, and stiffness (all tensile) properties. For the case analyzed here, which involves a relatively high concentration of sheet stacking faults (one sheet stacking fault for every 10 sheets), the results obtained show that the cross-sheet transverse tensile strength is lowered by 30%, and the cross-sheet transverse tensile ductility is lowered by ca. 33%. On average, the longitudinal and in-sheet strength, ductility, and stiffness were affected by less than 10%. The following Young's moduli were, respectively, obtained in this case: E_1 = 190 GPa, E_{22} = 14 GPa, and E_{33} = 6 GPa.

An example of the typical molecular-level configuration obtained in this case is displayed in Fig. 9(a) and (b). The results displayed in these figures correspond, respectively, to the case of a perfect PPTA crystal, Fig. 9(a), and a PPTA crystal containing a sheet stacking fault, Fig. 9(b), both subjected to the same cross-sheet transverse tensile load. It is evident that owing to the locally increased inter-sheet space, the defective material is less stiff/strong than its perfectly crystalline counterpart in the cross-sheet transverse direction.

4.5 Final Remarks

The results obtained in this study clearly revealed that the different microstructural/morphological defects could have profound effects on the mechanical properties of the PPTA crystalline fibers. This finding could have been expected since deviations from the perfect crystalline structure typically result in a significant loss of material mechanical properties. Nevertheless, it is hoped that the findings reported in this article when combined with our on-going study can have a broader impact on improving the quality of coarser length-scale (e.g., yarn-level, fabric-level, etc.) material models for high-performance polymer fiber-reinforced composites. As discussed earlier, for this approach to yield broader benefits, it must be extended to include at least the following phenomena/concepts: (a) stochastic nature of the defect topology, location, and, concentration/density must be combined with this purely molecular-level investigation; (b) correlations among various defect stochastic parameters and the polymer chemistry, polymer synthesis, and fiber processing conditions must be established; and (c) the nature of the coarser length-scale(s) (i.e., yarn and fabric, in this case) material models should be taken into account so that the molecular-level computational results can be used to properly re-parameterize and enrich these models. Study is underway which addresses all these issues, and the outcomes of this study will be reported in a future article.

5. Summary and Conclusions

Based on the results obtained in this study, the following summary remarks and main conclusions can be drawn:

1. The effect of four microstructural and topological defects on the strength, ductility, and stiffness of *p*-phenylene terephthalamide, PPTA (i.e., generic Kevlar®) fibers/filaments is

studied using molecular-level computational methods and tools.

2. The four defects considered include chain ends, inorganic-solvent impurities, chain misalignments, and sheet stacking faults. These defects are expected to be most prevalent in commercial PPTA-based fibers and are a result of the finite molecular weight of the chains, and the presence of non-ideal polymer/synthesis and fiber-processing conditions.
3. While the presence of these defects decreases all the mechanical properties of PPTA fibers, specific properties are found to be particularly sensitive to the presence of certain defects. For example, longitudinal tensile properties are found to be the most sensitive to the presence of chain ends, in-sheet transverse properties to the presence of chain misalignments, and cross-sheet transverse properties to the presence of sheet stacking faults.

Acknowledgments

The material presented in this article is based on study supported by the Army Research Office (ARO) research contract entitled "*Multi-length Scale Material Model Development for Armor-grade Composites*," Contract Number W911NF-09-1-0513, and the Army Research Laboratory (ARL) research contract entitled "*Computational Analysis and Modeling of Various Phenomena Accompanying Detonation Explosives Shallow-Buried in Soil*" Contract Number W911NF-06-2-0042. The authors are indebted to Bruce LaMattina of ARO for his continuing support and interest in this study.

References

1. M. Grujicic, B. Pandurangan, K.L. Koudela, and B.A. Cheeseman, A Computational Analysis of the Ballistic Performance of Light-Weight Hybrid-Composite Armor, *Appl. Surf. Sci.*, 2006, **253**, p 730–745
2. M. Grujicic, T. He, H. Marvi, B.A. Cheeseman, and C.-F. Yen, A Comparative Invesigation of the Use of Laminate-Level Meso-Scale and Fracture-Mechanics Enriched Meso-Scale Composite-Material Models in Ballistic Resistance Analyses, *J. Mater. Sci.*, 2010, **45**(12), p 3136–3150
3. M. Grujicic, D.C. Angstadt, Y.-P. Sun, and K.L. Koudela, Micro-Mechanics Based Derivation of the Materials Constitutive Relations for Carbon Nanotube Reinforced Poly-Vinyl-Ester-Epoxy Based Composites, *J. Mater. Sci.*, 2007, **42**, p 4609–4623
4. M. Grujicic, G. Arakere, T. He, M. Gogulapati, and B.A. Cheeseman, A Numerical Investigation of the Influence of Yarn-Level Finite-Element Model on Energy Absorption by a Flexible-Fabric Armor During Ballistic Impact, *J. Mater. Des. Appl.*, 2008, **222**, p 259–276
5. M. Grujicic, W.C. Bell, G. Arakere, T. He, X. Xie, and B.A. Cheeseman, Development of a Meso-Scale Material Model for Ballistic Fabric and Its Use in Flexible-Armor Protection Systems, *J. Mater. Eng. Perform.*, 2010, **19–1**, p 22–39
6. M. Grujicic, W.C. Bell, T. He, and B.A. Cheeseman, Development and Verification of a Meso-Scale Based Dynamic Material Model for Plain-Woven Single-Ply Ballistic Fabric, *J. Mater. Sci.*, 2008, **43**, p 6301–6323
7. B.A. Cheeseman, C.F. Yen, B.R. Scott, B. Powers, T.A. Bogetti, B. LaMatina, Y. Duan, M. Keefe, Y. Miao, and Y. Wang, "From Filaments to Fabric Packs—Simulating the Performance of Textile Protection Systems," ARL Report ADM002075, 2006
8. G.C. Rutledge and U.W. Suter, Detailed Atomistic Simulations of Oriented Pseudocrystalline Polymers and Applications to a Stiff Chain Aramid, *Macromolecules*, 1991, **24**, p 1924–1933
9. H.G. Chae and S. Kumar, Making Strong Fibers, *Science*, 2008, **319**, p 908–909
10. V.B. Gupta and V.K. Kothari, *Manufactured Fibre Technology*, Chapman & Hall, New York, 1997
11. M. Panar, P. Avakian, R.C. Blume, K.H. Gardner, T.D. Gierke, and H.H. Yang, Morphology of Poly(*p*-phenylterepthalamide) Fibers, *J. Polym. Sci.*, 1983, **21**, p 1955–1969
12. H. Sun, COMPASS: An Ab Initio Force-Field Optimized for Condensed-Phase Applications-Overview with Details on Alkane and Benzene Compounds, *J. Phys. Chem. B.*, 1998, **102**, p 7338
13. H. Sun, P. Ren, and J.R. Fried, The Compass Force Field: Parameterization and Validation for Phosphazenes, *Comput. Theor. Polym. Sci.*, 1998, **8**(1/2), p 229
14. http://www.accelrys.com/mstudio/msmodeling/visualiser.html
15. M. Grujicic, Y.P. Sun, and K.L. Koudela, The Effect of Covalent Functionalization of Carbon Nanotube Reinforcements on the Atomic-Level Mechanical Properties of Poly-vinyl-ester-epoxy, *Appl. Surf. Sci.*, 2007, **253**(2007), p 3009
16. http://www.accelrys.com/mstudio/msmodeling/discover.html
17. G.C. Rutledge and U.W. Suter, Calculation of Mechanical Properties of Poly(*p*-phenylene terephthalamide) by Atomistic Modelling, *Polymer*, 1991, **32**, p 12